Schrödinger-type traps for Lamb waves in dynamic potential wells

Xiangen Liu and Zhonghua Shen*
School of Science, Nanjing University of Science and Technology, Nanjing 210094, China

Alexey M. Lomonosov
Scientific and Technological Center for Unique Instrumentation, Russian Academy of Sciences, 117342 Moscow, Russian Federation

(Received 22 March 2024; revised 23 May 2024; accepted 7 June 2024; published 10 July 2024)

A dynamic trapping of Lamb modes with a frequency cutoff was achieved through local heating of an elastic plate using a cw laser. The relatively small variations in material stiffness resulting from the temperature rise proved effective at capturing waves within the heated region, which behaved like a potential well for specific Lamb modes. These trapped modes corresponded precisely to discrete frequencies predicted by the time-independent Schrödinger equation, reminiscent of the principle quantum number. The number of trapped modes hinges on both the width and depth of the laser-induced thermal potential well, with these variables interrelated via Heisenberg's uncertainty principle. Furthermore, we observed a high-quality factor (Q factor of approximately 260) attributed to the trapped wave motion within the potential well, offering significant promise for highly precise nondestructive evaluation of thermal and mechanical properties of materials.

DOI: 10.1103/PhysRevApplied.22.014022

I. INTRODUCTION

Trapped modes, referred to as bound states in the continuum of quantum mechanics, are characterized by their strong localization within unbounded media, despite coexisting with a continuous spectrum of radiating waves capable of carrying energy away [1]. From a mathematical perspective, the phenomenon of trapped modes in waveguides suggests the presence of a discrete spectrum of natural frequencies, accompanied by eigenfunctions strongly localized in the vicinity of inclusions (inhomogeneities) within the waveguide [2]. The study of trapped modes finds applications across a spectrum of fields, encompassing acoustics, photonics, and quantum mechanics. Profound insights into these modes and their manipulation can give rise to intriguing phenomena and pave the way for the development of innovative devices and technologies.

The phenomenon of energy trapping was first observed by Bechmann and Wigner in 1929 [3]. Since then, trapped modes have been recognized as a widespread wave phenomenon and have been identified in various wave systems. Trapped modes have been extensively studied and observed in electromagnetic waves, particularly in photonic structures where light can be confined within specific regions or structures [4,5]. Additionally, trapped modes have been investigated in acoustic waves propagating through air, leading to the discovery of localized resonant modes that exhibit strong confinement and long lifetimes [6,7]. In the context of water waves, trapped modes have been experimentally observed and analyzed, revealing localized wave patterns that persist in specific regions despite the presence of surrounding waves [8]. Furthermore, trapped modes have been identified and studied in elastic waves propagating through solid materials. The existence and properties of these localized modes have been explored, offering insights into wave localization and energy confinement in solids [9].

The trapped modes in acoustics and elastic waves find wide-ranging applications, such as wave manipulation [10] and control [11], nondestructive detection [12], resonant devices [7,13,14], wave isolation [15], and absorption [16]. Various methods exist to induce trapped modes in continuum waveguides, including introducing geometry variations, obstacles, and locally perturbing the elasticity of the medium. The existence of trapped modes in locally perturbed acoustic waveguides was initially observed experimentally by Parker in Ref. [17] and theoretically calculated in Ref. [18]. Evans further provided mathematical proof that any symmetric obstacle positioned on the centerline in an acoustical waveguide with Neumann boundary conditions could induce trapping modes [19–21]. Analogously, Porter provided numerical evidence for the existence of trapped modes on a thin elastic plate with a circular hole cut out of the centerline of the strip [22]. For locally induced trapped modes by variations in geometry, Johnson and Auld, among others, theoretically and

*Contact author: shenzh@njust.edu.cn

experimentally investigated torsional trapped modes in solid cylinders with locally larger-diameter central sections [23]. Maksimov conducted numerical studies on the existence of trapped modes in L-shaped, T-shaped, and X-shaped elastic waveguides with Dirichlet boundary conditions [24]. Postnova investigated trapped modes in both two-dimensional (2D) [25] and three-dimensional (3D) [26] elastic waveguides with topographical thickness variation by an asymptotic method. Wang conducted studies on the existence and characteristics of trapped modes in infinite or semi-infinite membrane strips with local enlargements [27]. Besides local enlargements, trapped modes may also occur in the vicinity of a local increase in density. Wang [28] further investigated the existence of trapped modes in membrane strips with a segment of higher density. Li investigated the occurrence of trapped modes in a cylindrical tube with a segment of higher density, which induced symmetric and antisymmetric trapped modes in the structure [29]. This study provided insights into the behavior of trapped modes in cylindrical structures with localized changes in density. Certainly, Yang *et al*. [30] designed an embedded inner plate consisting of material with a wave velocity lower than that of its outer plate and theoretically studied the trapped modes in such a structure. Additionally, trapped modes were also demonstrated to exist in elastic media of bent rods [31] and plates [31], plates with welded joints [12], and inner cracks [32]. Note that trapping effects due to local thickness variations and local curvature also occur in quantum waveguides [33–36]. A comprehensive review of the physical mechanisms, experimental studies, and applications of trapped modes across various material systems and in different types of waves is available in Ref. [37].

The preceding discussions have primarily centered on permanent trapping effects, where the occurrence, resonance frequency, and energy confinement of the trapped modes remain fixed, despite their crucial importance in wave manipulation and resonance devices. In this study, we introduce a method to dynamically trap elastic waves in a plate by heating it with a cw laser. It was discovered that modes with frequencies slightly lower than the A_1 cutoff can be localized in the heated area, where the temperature is higher than in the surrounding regions. This dynamic trapping mechanism enables tunable control over the trapped modes in the plate. To describe the A_1 trapped modes induced by thermal loading, a time-independent Schrödinger-type equation (TISE) was derived. This equation provides a mathematical framework for studying the behavior of trapped waves in the heated plate. The validity of the TISE was confirmed by solving the eigenvalue problem for the locally heated plate through numerical finite-element-method (FEM) calculations. The results derived from the application of the Schrödinger-type equation exhibited a remarkable consistency with the results obtained from both the FEM simulations and experimental measurements.

II. OBSERVATION OF SCHRÖDINGER-TYPE TRAPPED MODES

The experimental setup for investigating the elastic trapped modes induced by the thermal gradient is schematically depicted in Fig. 1(a). The sample utilized in this study is composed of an aluminum alloy with a thickness of 0.34 mm. Elastic trapped modes induced by the thermal gradient are investigated experimentally using laser ultrasonics (LUS) technique combined with fiber laser heating, with a radius of 2 mm on the sample surface. To detect and measure the resulting acoustic waves, a laser Doppler vibrometer (LDV) is employed. In the experimental setup, a nanosecond laser is employed to launch acoustic waves in the sample following a 1.2-s laser irradiation period. Subsequently, these waves are detected and measured using a laser Doppler vibrometer, facilitating the analysis of the trapped modes induced by the thermal gradient and the characterization of their properties. Figure 1(b) illustrates the temporal signal recorded at ambient temperature. The insets of Fig. 1(b), labeled as (i1) and (i2), offer enlarged plots depicting the temporal oscillation and spectrum, respectively, of the recorded signal at ambient temperature. The experiment details and the signal process can be found in the Supplemental Material [38]. Figure 1(c) specifically illustrates the spectra obtained at a heating power of 15 W and various other power levels. The spectrum extracted at a low heating power, where no resonance is observed around the cutoff of the A_1 mode, suggests that the trapped modes induced by the thermal gradient do not exhibit resonant behavior within this power range. As the heating power increases, one, two, and eventually three resonances are observed in the spectra. These resonances represent distinct frequency peaks or modes that are excited and trapped within the sample due to the stronger thermal gradient created by higher heating powers. Quality factor of the resonance is estimated to be approximately 260. The detection of multiple resonances with increasing heating power provides valuable insights into the tunability and control of trapped modes through dynamic heating in the experimental setup. It underscores the capability to manipulate the wave behavior and resonance characteristics of the system by adjusting the heating power applied via the cw laser. Figure 1(d) illustrates the power scanning of the spectrum across the cutoff of the A_1 mode. The frequencies of all three detected resonances in the spectrum originate from the cutoff of the A_1 mode; meanwhile, the frequency of each peak decreases with the increase of heating power. These resonances are referred to as the A_1 trapped mode and could be mathematically described using a time-independent Schrödinger-type equation (TISE) with

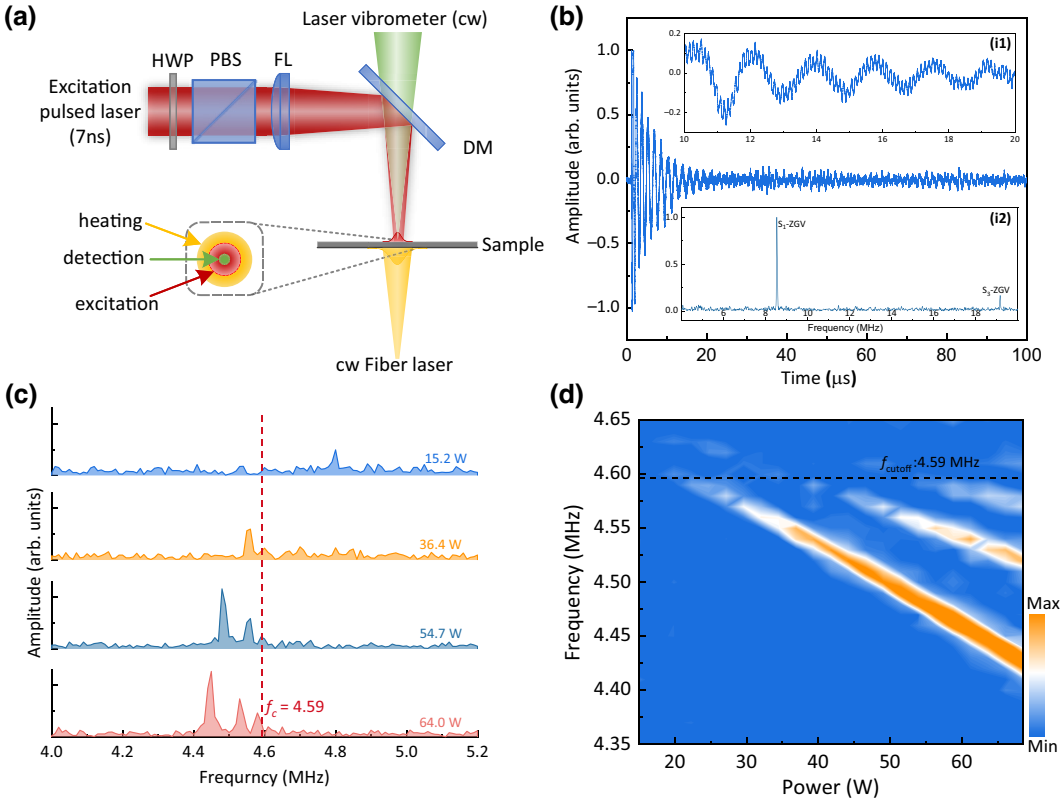

FIG. 1. (a) Experimental arrangements for excitation and detection of locally heating-induced trapped modes. HWP, half-wave plate; PBS, polarized beam splitter; FL, focal lens with a focal length of 40 centimeters; DM, dichroic mirror; cw, continuous wave. (b) Temporal signal recorded at ambient temperature. Insets: (i1) enlarged plot of the oscillating signal; (i2) Fourier spectrum of the signal; (c) Fourier spectrum of the acoustic signal recorded under different heating powers; (d) variations of the spectrum with laser heating power.

a wave function exhibiting similarities to that of a particle in a potential well.

III. TISE FOR A_1 TRAPPED MODES

The homogeneous elastic plate supports two types of waves propagating parallel to the plate: symmetric and antisymmetric modes, denoted as S_n and A_n, respectively, with $n = 0, 1, 2, \ldots$. The two lowest antisymmetric modes, A_0 and A_1, are depicted in Figure 2. Here, the blue curves represent the dispersion of the modes outside the heated area, while the pink curves correspond to the center of the heated region, where frequencies are reduced. Notably, the modes with $n = 0$ exist across the entire frequency range, spanning from zero to extremely high frequencies. Modes with nonzero n possess what is called a cutoff frequency: their frequency range is limited at the low end by the thickness resonances f_c of either longitudinal or transverse waves. Below the cutoff frequency, these modes exist in the form of evanescent waves with an imaginary (or sometimes complex-valued) wave number k, depicted by dashed curves. The cutoff frequency of the antisymmetric A_1 Lamb mode is determined by the half-wave resonance of the shear wave as $\omega_c = 2\pi f_c = \pi V_S/2h$, where h represents half of the plate thickness. In the area of local heating, the shear velocity $V_{S,T}$, and hence the cutoff frequency $\omega_{c,T}$, are smaller than those in the surrounding area. As a result, the wave with a frequency in the range $f_{c,T} < f < f_c$ possesses a real-valued wave vector k in the hot area, but outside the wave becomes evanescent with imaginary k, as indicated in Fig. 2. Evanescent waves do not transmit energy, so the mode remains trapped. It is worth noting that the transition from propagating to evanescent wave is a characteristic feature of the time-independent Schrödinger equation: for waves with energy (or frequency) less than the well depth, k is real inside the well and imaginary (or complex) outside. Note that the possible coupling of the trapped A_1 mode with the A_0 mode in the surrounding cold region is inefficient because the wave-number ranges of the two modes do not overlap, as seen in Fig. 2. The trapped mode has $|k| < 25\,\mathrm{cm}^{-1}$, whereas the A_0 mode of the same frequency has $|k| \approx 100\,\mathrm{cm}^{-1}$.

Here, we demonstrate that the TISE can serve as a good approximation for the A_1-type Lamb wave trapped in a compact hot area. The displacement field of the acoustic wave in a solid can be conveniently expressed in terms of

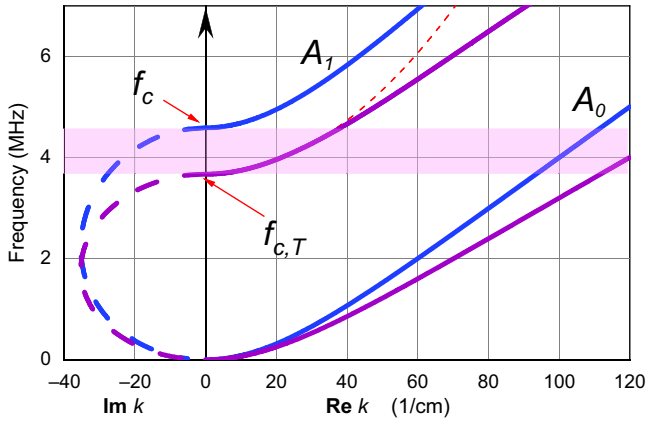

FIG. 2. Dispersion curves of the first two antisymmetric modes; blue lines are dispersion curve of Lamb wave in ambient temperature while purple lines are that under temperature increase.

the scalar and vector potentials

$$\mathbf{u}(\mathbf{r},t) = \vec{\nabla}F(\mathbf{r},t) + \vec{\nabla} \times \mathbf{H}(\mathbf{r},t) \tag{1}$$

supplemented by the requirement $\vec{\nabla} \cdot \mathbf{H} = 0$. In these terms the equation of motion for the homogeneous solid splits into two independent equations for F and $\mathbf{H}$:

$$V_L^2 \Delta F = \frac{\partial^2}{\partial t^2} F = -\omega^2 F, \tag{2a}$$

$$V_S^2 \Delta \mathbf{H} = \frac{\partial^2}{\partial t^2} \mathbf{H} = -\omega^2 \mathbf{H}, \tag{2b}$$

where V_L and V_S denote the longitudinal and shear waves velocities, respectively.

Here, we assume an axially symmetric spatial variation of both velocities: $V_{S,L} = V_{S,L}(r)$, induced by the local temperature $T(r)$. In a plate, the traction-free boundary conditions at the surfaces $z = \pm h$ are met through the superposition of shear and longitudinal waves propagating at specific angles to the plate normal, while sharing the same lateral component of the k vector. This superposition forms the Lamb wave with wave vector k, and establishes a rigid relationship between the potentials F and $\mathbf{H}$. Since in the small-k region the A_1 mode is primarily shear, the contribution of the vector potential dominates, allowing us to focus on Eq. (2b). Because of the axial symmetry, in the cylindrical symmetric coordinates (r, θ, z), the angular dependence of all variables vanishes, resulting in only the H_θ component being nonzero. Equation (2b) is then reduced to $H_\theta = H(r,z)$ and takes the following form:

$$V_S^2 \left(\frac{\partial^2 H}{\partial r^2} + \frac{1}{r}\frac{\partial H}{\partial r} - \frac{1}{r^2} H \right) + V_S^2 \frac{\partial^2 H}{\partial z^2} + \omega^2 H = 0. \tag{3}$$

For Lamb waves, the z dependence has a generally harmonic form $Z(z) \sim 1 + c\exp(ik_z z)$, with constant c necessary to satisfy the free-boundary conditions at the plate surfaces. Then $H(r,z) = h(r)Z(z)$, and $\frac{\partial^2}{\partial z^2} = -k_z^2$See (see Supplemental Material [38]). At a given ω, the radial components of the wave vectors of F and H are equal:

$$\frac{\omega^2}{V_L^2} - k_{L,z}^2 = \frac{\omega^2}{V_S^2} - k_{S,z}^2 = k^2. \tag{4}$$

The radial wave number k is related to ω by the Lamb equation. In the small-k limit, the dispersion relation for waves with cutoff, such as the A_1 Lamb mode, can be approximated to the quadratic term as

$$\begin{aligned} \omega &= \frac{\pi V_S}{2h} + \frac{hV_S}{\pi}\left(1 + \frac{16}{\pi}\frac{V_S}{V_L}\cot(\frac{\pi}{2}\frac{V_S}{V_L})\right)k^2 + \cdots \\ &= \omega_c + Ak^2 + \cdots \end{aligned} \tag{5}$$

For simplicity, we assume that the temperature dependence of V_S and V_L follows the same expression approximately $(1 - \alpha T)$ (see Supplemental Material [38], including Refs. [39,40]), where α represents the same coefficient for both velocities. From Eq. (5), it follows that the parameter

$$A = \frac{hV_S}{\pi}\left(1 + \frac{16}{\pi}\frac{V_S}{V_L} ctg\left(\frac{\pi}{2}\frac{V_S}{V_L}\right)\right)$$

also varies with T and r as $A = a(1 - \alpha T(r))$. Taking into account the smallness of $\alpha T(r)$, the spatial-dependent dispersion relation can be approximated as

$$k^2 = \frac{1}{a}(\omega - \omega_c(r)) \tag{6}$$

to the first order in αT, as shown by the dashed red curve in Fig. 2. Below ω_c, the Lamb mode becomes evanescent with imaginary k, represented by the blue dashed line. Utilizing Eqs. (4) and (6) in Eq. (3) yields the time-independent Schrödinger-type equation for the radial component of the vector potential $h(r)$:

$$\left(\frac{d^2h}{dr^2} + \frac{1}{r}\frac{dh}{dr} - \frac{h}{r^2}\right) + \left(\frac{\omega}{a} - \frac{\omega_c(r)}{a}\right)h = 0. \tag{7}$$

The potential well $V(r)$ is determined by the term $V(r) = \omega_c(r)/a$. The coefficient of h plays a role of k^2; outside the potential well, it becomes negative, resulting in an imaginary k. As a consequence, the wave cannot propagate in that region and remains trapped. Solutions of Eq. (7) that tend to 0 as $r \to \infty$, only exist for specific discrete values of $\omega_k/a = E_k$. These values represent the eigenvalues of the Schrödinger equation with zero boundary conditions.

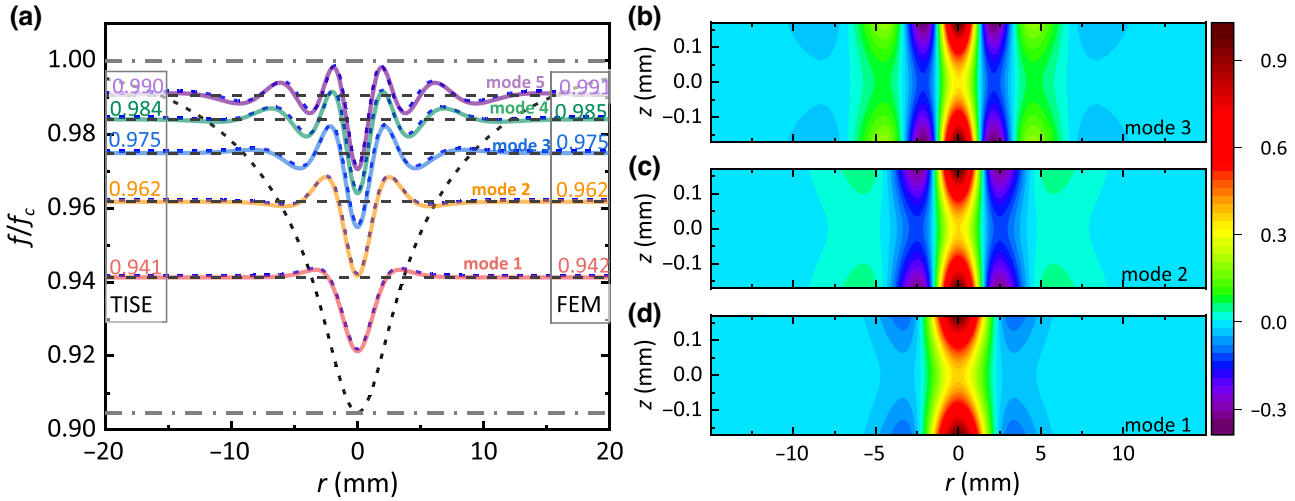

FIG. 3. (a) Dashed black line: distribution of the potential well induced by the local laser heating given by Eq. (9); solid colored curves: U_z of the trapped modes calculated by the TISE model, and dashed colored curves are those from the FEM simulation; (b)–(d) color denotes the $U_z(z,r)$ amplitudes of the first three trapped modes shown in (a) calculated by FEM.

The out-of-plane displacement that was measured in the experiment is given by

$$U_z(r,t) = \left(\frac{dh}{dr} + \frac{h}{r}\right)\exp(i\omega_k t). \tag{8}$$

In the experiment, the spatial inhomogeneity of V_S, V_L, and ω_c resulted from local heating by a cw laser focused into a circular Gaussian spot with a radius of b on the surface, so that the heat flux inward into the sample was approximately $\exp(-r^2/b^2)$. The temperature distribution across the plate thickness can be considered uniform if $\sqrt{tD} \gg h$, where D represents the thermal diffusivity and t is the heating time. Under this approximation, the solution to the heat equation is given by

$$T(r,t) \sim \frac{b^2}{4D}\left(E_1\left(\frac{r^2}{b^2+4Dt}\right) - E_1\left(\frac{r^2}{b^2}\right)\right), \tag{9}$$

where $E_1(x)$ is the first exponential integral, defined as $\int_x^\infty \exp(-s)/s\,ds$ for $x > 0$.

The potential well, generated by the temperature distribution (9) with a power flux of 60 W absorbed at the spot with a radius of $b = 2$ mm after heating for 1 s, is depicted in Fig. 3 by the black dashed bell-shaped curve. The potential well is bounded by the two gray horizontal dash-dot lines. The upper limit corresponds to the unperturbed cutoff frequency for the A_1 mode with $\omega_c = \pi V_S/2h$, while the lower limit is determined by the maximal temperature in the center, given by $\omega = \omega_c(1-\alpha T)$. The eigenvalues of Eq. (7) within the thermal-induced potential well, as depicted in Fig. 3, along with the corresponding waveforms, have been numerically computed using the Numerov method [41] modified for cylindrical coordinates [42]. The temperature increase at the center reached 280 K, resulting in a 9% change in the shear and longitudinal velocities and the cutoff frequency. This level of inhomogeneity was sufficient to trap at least five localized states with frequencies 0.94, 0.96, 0.975, 0.984, and 0.99 of the resonance frequency in the cold region. The five solutions (depicted by solid curves) localized in the well exhibit behavior typical of Schrödinger solutions, with real k and oscillatory character inside the well, and exponential decay outside.

The validity of Eq. (7) was confirmed through numerical FEM calculations solving the eigenvalue problem for the locally heated plate (see the Supplemental Material [38]). Figure 3(a) compares the U_z waveforms and eigenfrequencies obtained from Eq. (8) (shown by solid colored curves) and by FEM (dashed colored curves). From Fig. 3, it is apparent that the one-dimensional TISE provides a precise approximation of the 3D wave field in terms of U_z at the surface and frequencies. Figures 3(b)–3(d) depict the FEM simulation mode shapes of the first three trapped modes shown in Fig. 3(a). As the trapped modes originate from the A_1 mode, the displacement across the thickness remains similar to that in the conventional A_1 mode, while the lateral distribution is precisely described by the Schrödinger wave function.

In the experiment only three peaks have been observed. We ascribe that to the effect of the sample holder on the spatial temperature distribution. In this scenario, the temperature change at the radius of the holder can be approximated as $T(r_0) = 0$, with $r_0 = 7$ mm. The solution of the heat equation approaches the stationary distribution

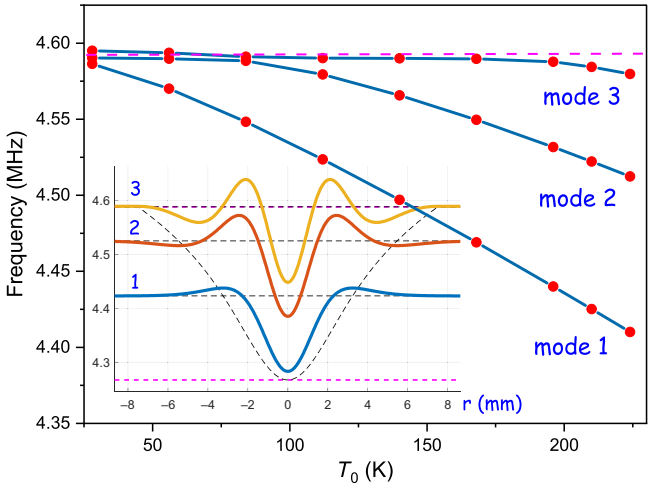

FIG. 4. Temperature dependence of A_1 trapped modes. Inset: U_z displacement amplitudes of the three trapped modes at the maximum heating in the temperature field given by Eq. (10).

after approximately 0.7 s, as given by

$$T(r < r_0) = \frac{W}{4\pi D}\left(E_1\left(\frac{r_0^2}{b^2}\right) - E_1\left(\frac{r^2}{b^2}\right) + \ln\left(\frac{r_0^2}{r^2}\right)\right),$$
$$T(r > r_0) = 0. \tag{10}$$

The temperature distribution and corresponding solutions to the Schrödinger equation are illustrated in Fig. 4. The waveforms of the three trapped modes, consistent with the first three modes in Fig. 3(a), are depicted in the inset of Fig. 4. The temperature dependence of the three trapped modes shown in Fig. 4 aligns well with the experimental measurements in Fig. 1(d). This correspondence indicates that the TISE [Eq. (7)] and the thermal potential well induced by Eq. (10) are appropriate for describing the A_1 trapped modes in the locally heated area.

Modes trapped within the potential well adhere to specific size-frequency relations, analogous to the Heisenberg uncertainty relations known for Schrödinger solutions. The mean square radius of the trapped mode can be calculated as

$$\langle r^2 \rangle = 2\pi \int_0^\infty r^2 \psi^2(r) r\, dr, \tag{11}$$

where functions $\psi(r)$ are the normalized eigenfunctions of the Schrödinger equation (7), so that

$$\psi(r) = \frac{h(r)}{2\pi \int_0^\infty h^2(r) r\, dr}$$

. Momentum we introduce formally as $p = i\partial/\partial r$, which is proportional to k. Mean square momentum is calculated as

$$\langle p^2 \rangle = -2\pi \int_0^\infty \psi(r) \Delta\psi(r) r\, dr. \tag{12}$$

For each trapped mode $\psi_n(r)$ the product $\langle r^2 \rangle \langle p^2 \rangle$ is independent of the specific shape or depth of the potential well; it is solely determined by n:

$$\sqrt{\langle r_n^2 \rangle \langle p_n^2 \rangle} = 2n. \tag{13}$$

This is analogous to the Heisenberg uncertainty relation, where the sequential number of the mode n serves as the principle quantum number.

IV. CONCLUSION

In summary, this study presents a dynamic trapping mechanism induced by locally heating an elastic plate to capture the A_1 Lamb mode, and more generally, any mode with the frequency cutoff. The eigenfrequencies of such a trap are determined not only by the size of the heated area, like in resonators, but mostly by the shape of the temperature distribution. Quantitatively, this behavior is analogous to the eigenmodes of a quantum particle in a potential well, as described by the Schrödinger equation. In our experiments the "potential well" appeared as a result of softening of solid in the region heated by a cw laser. The depth and width of such a potential well can be easily tuned by varying the size of the laser spot, the power, and the duration of heating. Experiments and FEM simulations validated the theoretical TISE model, accurately reproducing the shapes and frequencies of the trapped modes. Additionally it was shown, that the trapped modes obey the uncertainty relations, similar to those known for the Schrödinger solutions, known as the Heisenberg uncertainty principle.

The data that support the findings of this study are available from the contact author upon reasonable request.

ACKNOWLEDGMENTS

This work was supported by the National Natural Science Foundation of China (Grant No. 61975080) and the Funding of NJUST (Grant No. TSXK2022D00x).

X.L. experiment conducting, data processing, writing; A.L. methodology, programming, data processing, writing; Z.S. methodology, supervision, writing. X.L and A.L contributed equally to this work.

The authors have no conflicts to disclose.

[1] M. A. Langthjem and M. Nakano, On the acoustic trapped modes and their symmetry properties in a circular cylindrical waveguide with a cavity, J. Eng. Math. **128**, 14 (2021).

[2] J. D. Kaplunov and S. V. Sorokin, A simple example of a trapped mode in an unbounded waveguide, J. Acoust. Soc. Am. **97**, 3898 (1995).

[3] J. V. Neumann and E. Wigner, Über merkwürdige diskrete eigenwerte, Phys. Z **30**, 291 (1929).

[4] A. Kodigala, T. Lepetit, Q. Gu, B. Bahari, Y. Fainman, and B. Kanté, Lasing action from photonic bound states in continuum, Nature **541**, 196 (2017).

[5] C. W. Hsu, B. Zhen, J. Lee, S.-L. Chua, S. G. Johnson, J. D. Joannopoulos, and M. Soljačić, Observation of trapped light within the radiation continuum, Nature **499**, 188 (2013).

[6] N. A. Cumpsty and D. Whitehead, The excitation of acoustic resonances by vortex shedding, J. Sound Vib. **18**, 353 (1971).

[7] B. Jia, L. Huang, A. S. Pilipchuk, S. Huang, C. Shen, A. F. Sadreev, Y. Li, and A. E. Miroshnichenko, Bound states in the continuum protected by reduced symmetry of three-dimensional open acoustic resonators, Phys. Rev. Appl. **19**, 054001 (2023).

[8] P. Cobelli, V. Pagneux, A. Maurel, and P. Petitjeans, Experimental observation of trapped modes in a water wave channel, Europhys. Lett. **88**, 20006 (2009).

[9] V. Pagneux, in *Dynamic Localization Phenomena in Elasticity, Acoustics and Electromagnetism* (Springer, Berlin, 2013), p. 181.

[10] S. Xie, H. Ding, Z. Zhou, Y. Li, and T. Hao, Wideband subwavelength acoustic edge detection via trapped modes with breaking structural periodicity, Appl. Phys. Express **15**, 084002 (2022).

[11] I. Quotane, E. H. E. Boudouti, and Bahram Djafari-Rouhani, Trapped-mode-induced Fano resonance and acoustical transparency in a one-dimensional solid-fluid phononic crystal, Phys. Rev. B **97**, 024304 (2018).

[12] W. Li, Z. Lan, N. Hu, and M. Deng, Theoretical and numerical investigations of the nonlinear acoustic response of feature guided waves in a welded joint, Wave Motion **101**, 102696 (2021).

[13] F. Zhu, P. Li, X. Dai, Z. Qian, I. E. Kuznetsova, V. Kolesov, and T. Ma, A theoretical model for analyzing the thickness-shear vibration of a circular quartz crystal plate with multiple concentric ring electrodes, IEEE Trans. Ultrason. Ferroelectr. Freq. Control **68**, 1808 (2020).

[14] L. Huang, Y. K. Chiang, S. Huang, C. Shen, F. Deng, Y. Cheng, B. Jia, Y. Li, D. A. Powell, and A. E. Miroshnichenko, Sound trapping in an open resonator, Nat. Commun. **12**, 4819 (2021).

[15] S. Huang, T. Liu, Z. Zhou, X. Wang, J. Zhu, and Y. Li, Extreme sound confinement from quasibound states in the continuum, Phys. Rev. Appl. **14**, 021001 (2020).

[16] L. Cao, Y. Zhu, S. Wan, Y. Zeng, Y. Li, and B. Assouar, Perfect absorption of flexural waves induced by bound state in the continuum, Extreme Mech. Lett. **47**, 101364 (2021).

[17] R. Parker, Resonance effects in wake shedding from parallel plates: Some experimental observations, J. Sound Vib. **4**, 62 (1966).

[18] R. Parker, Resonance effects in wake shedding from parallel plates: Calculation of resonant frequencies, J. Sound Vib. **5**, 330 (1967).

[19] M. Callan, C. Linton, and D. Evans, Trapped modes in two-dimensional waveguides, J. Fluid Mech. **229**, 51 (1991).

[20] D. Evans, M. Levitin, and D. Vassiliev, Existence theorems for trapped modes, J. Fluid Mech. **261**, 21 (1994).

[21] D. Evans and R. Porter, Trapped modes about multiple cylinders in a channel, J. Fluid Mech. **339**, 331 (1997).

[22] R. Porter, Trapped waves in thin elastic plates, Wave Motion **45**, 3 (2007).

[23] W. Johnson, B. Auld, E. Segal, and F. Passarelli, Trapped torsional modes in solid cylinders, J. Acoust. Soc. Am. **100**, 285 (1996).

[24] D. N. Maksimov and A. F. Sadreev, Bound states in elastic waveguides, Phys. Rev. E **74**, 016201 (2006).

[25] J. Postnova and R. V. Craster, Trapped modes in topographically varying elastic waveguides, Wave Motion **44**, 205 (2007).

[26] J. Postnova and R. Craster, Trapped modes in 3d topographically varying plates, IMA J. Appl. Math. **73**, 950 (2008).

[27] C. Wang, Effect of local enlargement on the trapped modes of infinite or semi-infinite membrane strips, Mech. Res. Commun. **57**, 6 (2014).

[28] C. Wang, Vibration of a membrane strip with a segment of higher density: analysis of trapped modes, Meccanica **49**, 2991 (2014).

[29] W.-S. Li, K. Y. Lee, and X.-F. Li, Trapped modes in an infinite tube with inhomogeneity, Mod. Phys. Lett. B **34**, 2050060 (2020).

[30] Q. Yang, J. Liao, X. Fan, J. Luo, and C. Fu, Trapped degenerate modes in an embedded-core flat circular plate, J. Sound Vib. **552**, 117643 (2023).

[31] D. Gridin, A. Adamou, and R. Craster, Trapped modes in bent elastic rods, Wave Motion **42**, 352 (2005).

[32] R. Porter and D. V. Evans, Trapped modes due to narrow cracks in thin simply-supported elastic plates, Wave Motion **51**, 533 (2014).

[33] J. P. Carini, J. Londergan, K. Mullen, and D. Murdock, Bound states and resonances in waveguides and quantum wires, Phys. Rev. B **46**, 15538 (1992).

[34] G. Annino, H. Yashiro, M. Cassettari, and M. Martinelli, Properties of trapped electromagnetic modes in coupled waveguides, Phys. Rev. B **73**, 125308 (2006).

[35] P. Amore, M. Rodriguez, and C. A. Terrero-Escalante, Bound states in open-coupled asymmetrical waveguides and quantum wires, J. Phys. A: Math. Theor. **45**, 105303 (2012).

[36] S. Bittner, B. Dietz, M. Miski-Oglu, A. Richter, C. Ripp, E. Sadurni, and W. P. Schleich, Bound states in sharply bent waveguides: Analytical and experimental approach, Phys. Rev. E **87**, 042912 (2013).

[37] C. W. Hsu, B. Zhen, A. D. Stone, J. D. Joannopoulos, and M. Soljačić, Bound states in the continuum, Nat. Rev. Mater. **1**, 1 (2016).

[38] See Supplemental Material at http://link.aps.org/supplemental/10.1103/PhysRevApplied.22.014022 for experimental details and solutions for the thermal potential well.

[39] H. Ledbetter, Sound velocities, elastic constants: Temperature dependence, Mater. Sci. Eng.: A **442**, 31 (2006).
[40] Y. Varshni, Temperature dependence of the elastic constants, Phys. Rev. B **2**, 3952 (1970).
[41] Y. Onodera, Numerov integration for radial wave equations in cylindrical symmetry, Comput. Phys. **8**, 352 (1994).
[42] V. Giurgiutiu, *Structural Health Monitoring: with Piezoelectric Wafer Active Sensors* (Elsevier, Burlington, 2007).